Neuron
Article

Activity-Regulated N-Cadherin Endocytosis

Chin-Yin Tai,[1] Shreesh P. Mysore,[3] Cindy Chiu,[1] and Erin M. Schuman[1,2,*]
[1] Division of Biology 114-96
[2] Howard Hughes Medical Institute
California Institute of Technology, Pasadena, CA 91125, USA
[3] Department of Neurobiology, Stanford University School of Medicine, Stanford, CA 94305, USA
*Correspondence: schumane@its.caltech.edu
DOI 10.1016/j.neuron.2007.05.013

SUMMARY

Enduring forms of synaptic plasticity are thought to require ongoing regulation of adhesion molecules, such as N-cadherin, at synaptic junctions. Little is known about the activity-regulated trafficking of adhesion molecules. Here we demonstrate that surface N-cadherin undergoes a surprisingly high basal rate of internalization. Upon activation of NMDA receptors (NMDAR), the rate of N-cadherin endocytosis is significantly reduced, resulting in an accumulation of N-cadherin in the plasma membrane. β-catenin, an N-cadherin binding partner, is a primary regulator of N-cadherin endocytosis. Following NMDAR stimulation, β-catenin accumulates in spines and exhibits increased binding to N-cadherin. Overexpression of a mutant form of β-catenin, Y654F, prevents the NMDAR-dependent regulation of N-cadherin internalization, resulting in stabilization of surface N-cadherin molecules. Furthermore, the stabilization of surface N-cadherin blocks NMDAR-dependent synaptic plasticity. These results indicate that NMDAR activity regulates N-cadherin endocytosis, providing a mechanistic link between structural plasticity and persistent changes in synaptic efficacy.

INTRODUCTION

The reciprocal communication between pre- and postsynaptic compartments of excitatory synapses is important for the activity-dependent regulation of synaptic strength in both the developing and the adult nervous system. Synaptic adhesion molecules present in both pre- and postsynaptic neurons are ideal targets for activity-dependent signaling and regulation (reviewed by Yamagata et al., 2003). N-cadherin, the most extensively studied adhesion molecule at the synapse, connects pre- and postsynaptic membranes through Ca^{2+}-dependent homophilic interactions (reviewed by Murase and Schuman, 1999; Salinas and Price, 2005; Takeichi and Abe, 2005). Furthermore, N-cadherin is positioned to regulate the structure of synapses via interactions with actin filaments, cytoskeletal elements enriched at synapses. N-cadherin interacts with actin through its binding proteins, α- and β-catenins (among others) (reviewed by Bienz, 2005; Kosik et al., 2005). Disruption of N-cadherin function at synapses interferes with synaptic plasticity such as long-term potentiation (LTP) (Tang et al., 1998; Bozdagi et al., 2000). Furthermore, overexpression of a dominant-negative form of N-cadherin in cultured hippocampal neurons causes morphological changes in dendritic spines (Bozdagi et al., 2004; Okamura et al., 2004; Togashi et al., 2002). Manipulation of either α- or β-catenin results in significant structural changes in spines (Abe et al., 2004; Murase et al., 2002; Yu and Malenka, 2003). Thus, the cadherin/catenin adhesion complex plays an important role in regulating synaptic activity and structure.

The motility and morphology of dendritic spines is regulated by synaptic activity. Earlier work suggests that the abundance of adhesion molecules can constrain the morphological dynamics that may contribute to synaptic plasticity. For example, Bailey and coworkers observed that the application of serotonin stimulated endocytosis of an *Aplysia* cell adhesion molecule (apCAM) and new synaptic growth in *Aplysia* sensory neurons (Bailey et al., 1992). This result suggests that trafficking of adhesion molecules can be regulated by neural activity that is associated with structural remodeling.

The regulation of cadherin endocytosis has been described in nonneuronal cells, and members of the catenin family play an important role in this process (reviewed by Bryant and Stow, 2004; Le et al., 1999). In neurons, β-catenin colocalizes with N-cadherin at excitatory synapses (Benson and Tanaka, 1998) and moves preferentially into spines upon depolarization (Murase et al., 2002). Interestingly, N-cadherin acquires protease-resistant properties after synaptic stimulation, suggesting an increase in the population of stable N-cadherin after synaptic activation (Tanaka et al., 2000). This increased stability may be due to enhanced interactions with β-catenin upon stimulation. This idea is supported by an in vitro study demonstrating that the orderly formation of cadherin zipper requires the association of β-catenin (Huber et al., 2001). In neurons, depolarization promotes the association of β-catenin and N-cadherin in a tyrosine phosphorylation-dependent manner, linking neuronal activity to enhanced N-cadherin/β-catenin associations (Murase et al., 2002).

In the present study, we demonstrate that the endocytosis of N-cadherin is regulated by NMDAR-dependent neuronal activity. In addition, we find that β-catenin is a key mediator of this regulation. Upon NMDAR activation, β-catenin is concentrated in dendritic spines, increases its association with N-cadherin by remaining in the unphosphorylated state, and, as a result, stabilizes surface N-cadherin by decreasing its internalization. Furthermore, prolonged stability of N-cadherin abolishes long-term depression (LTD) induced by NMDAR activation. These results indicate that the NMDAR-dependent regulation of N-cadherin trafficking plays a crucial role in synaptic function and plasticity.

RESULTS

Surface N-Cadherin Undergoes Both Constitutive and Activity-Regulated Endocytosis

We examined the time course of surface N-cadherin endocytosis using a biotinylation and internalization assay in cultured hippocampal neurons (see Experimental Procedures). Surprisingly, we found that N-cadherin exhibited a high basal rate of endocytosis. Under control (untreated) conditions, N-cadherin endocytosis occurred with a time constant (τ) of 33.0 ± 7.2 min (control groups in Figures 1A and 1B). The constitutive endocytosis of N-cadherin reached a steady state after 100 min and, on average, 42.8% ± 3.4% of the surface population was internalized. We next addressed whether the internalization of N-cadherin can be regulated by glutamatergic receptor activation. A brief (3 min) activation of NMDAR with the selective agonist NMDA (20 μM) caused a nearly 2-fold reduction in the endocytic rate of N-cadherin (τ = 59.9 ± 8.2 min) (Figures 1A and 1B). In addition, the amount of internalized N-cadherin at 100 min decreased to 28.5% ± 4.8% ($p < 0.05$ relative to control at 100 min), indicating an ~1.5-fold reduction in the total amount of N-cadherin internalized. The effects of NMDA application were completely prevented by pretreatment with the NMDAR antagonist APV (100 μM) (τ = 36.5 ± 4.8 min, Figures 1A and 1B). The application of APV without NMDA did not significantly alter N-cadherin endocytosis rates (τ = 39.2 ± 5.4 min, Figures 1A and 1B). These results suggest that in the absence of stimulation, tonic activation of NMDAR does not regulate N-cadherin endocytosis rates. The enhancement of excitatory synaptic transmission elicited by application of a GABA receptor antagonist, bicuculline (50 μM), caused a similar reduction in N-cadherin endocytosis, suggesting the increased activity of synaptic NMDAR is sufficient for this regulation (see Figure S1 in the Supplemental Data). To assess whether the effects of NMDA represent a general modulation of constitutive endocytosis, we also examined the internalization of the transferrin receptor (TfR) of N-cadherin. NMDA application did not modulate the endocytosis of TfR (control, τ = 9.8 ± 2.3 min; +NMDA, τ = 10.9 ± 3.2 min, Figures 1A and 1B). Thus, NMDAR activation causes a specific reduction in the rate of N-cadherin endocytosis, leading to an increase in the amount of N-cadherin remaining on the cell surface.

In principle, the reduction in internalized N-cadherin detected following NMDA treatment could be due to increased intracellular proteolysis. This was not the case—the lysosomal protease inhibitor leupeptin was included in all experiments, and there was no significant difference in the amount of total N-cadherin protein between control and +NMDA groups (93.1% ± 3.1% versus 97.6% ± 4.5% relative to time zero, data not shown). These data suggest that NMDA treatment did not elicit a detectable degradation of N-cadherin protein by other proteases. We also tested whether the rate of internalized N-cadherin recycling (back to the surface) is accelerated in the NMDA treatment group, which would result in decreased detection of internalized N-cadherin in the endocytosis assays. We performed recycling assays with or without NMDA treatment. The time constants, reflecting the time at which the biotinylated and internalized population of N-cadherin returns back to the surface, for the +NMDA and control groups were not significantly different from one another (+NMDA, τ = 8.2 ± 2.4 min; control, τ = 9.8 ± 3.9 min, Figures 1C and 1D), indicating that the rate of recycling was not affected by NMDA treatment. We thus conclude that a decrease in the rate of N-cadherin endocytosis is primarily responsible for the retention of surface N-cadherin after NMDAR activation.

Surface N-Cadherin Accumulates at Both Extrasynaptic and Synaptic Sites after NMDA Treatment

We next examined whether NMDA treatment causes a redistribution of surface N-cadherin along the dendrites. To examine the localization of surface N-cadherin in intact dendrites, we generated a polyclonal antibody against the extracellular (EC) domains 3–5 of N-cadherin protein. In cortical extracts from adult rat brain, the antibody recognized a single 130 kDa species, which corresponds to the predicted size of N-cadherin (Figure 2A). In addition, depletion of N-cadherin-specific antibody from the total IgG abolished the recognition of the 130 kDa N-cadherin species (Figure 2A).

In order to determine whether NMDA affects the endocytosis of synaptic and extrasynaptic populations of N-cadherin, we conducted live N-cadherin antibody-labeling assays in neurons 1 hr after NMDA treatment (we confirmed the effectiveness of the NMDA treatment by observing both an increased internalization of GluR1 subunits and a decreased miniature excitatory postsynaptic current (mEPSC) frequency; see Figure S3, e.g., Beattie et al., 2000). Previous attempts to access the synaptic population (Blanpied et al., 2002) using live-labeling have failed (C.Y.T. and C.C., unpublished data). Interestingly, we found that we could reliably detect the surface N-cadherin population after the removal of extracellular calcium by EGTA treatment (Figure 2B and Figure S2), suggesting that the epitopes are only accessed after the disassembly of N-cadherin oligomers. Note that we have

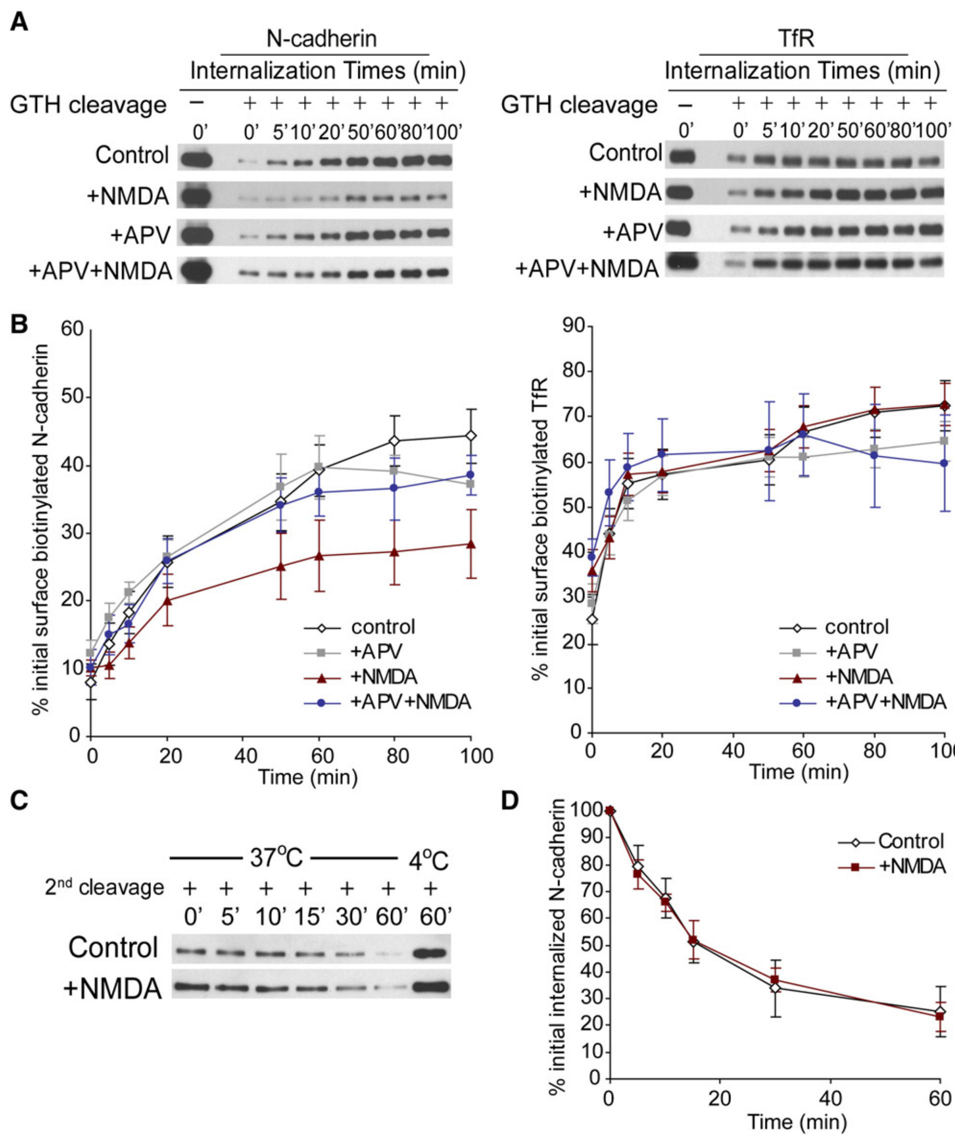

Figure 1. The Endocytosis of N-Cadherin Is Rapid and Regulated by NMDAR Activity

(A) Representative blots of N-cadherin internalization experiments in cultured hippocampal neurons. Surface proteins were labeled with biotin (as described in the Experimental Procedures), treated with NMDA (20 μM, 3 min at 37°C), and then returned to the incubator. After incubation for variable times (internalization times), the residual extracellular biotin groups were removed by glutathione (GTH) treatment. Transferrin receptor (TfR) was used as a control, representing constitutive endocytosis. NMDA treatment caused a reduction in N-cadherin internalization.

(B) Summary plot (mean ± SEM, n = 9, 8, 8, 5 for Control, +NMDA, +APV and +APV+NMDA, respectively).

(C and D) The recycling rate of the internalized N-cadherin was not affected by NMDA treatment (mean ± SEM, n = 5). A set of control experiments (right lane) was performed at 4°C to prevent recycling; the internalized protein remained inside the cell and thus spared the biotin groups of internalized proteins from the second cleavage. (N-cadherin control versus NMDA, $p < 0.01$; ANOVA with Tukey-Kramer's post hoc comparisons).

extensively characterized the effects of EGTA treatment on membrane integrity and total N-cadherin signal intensity (Figure S2). To analyze the synaptic population, we examined the N-cadherin signal that overlapped with the presynaptic marker bassoon (Figure 2C). Analysis of deconvolved N-cadherin particles revealed an ~26% increase in the mean intensity of total surface N-cadherin in the NMDA treatment group relative to control (Figures 2C and 2D). (The mean intensity of bassoon did not differ between groups). The increase in the surface N-cadherin mean intensity was observed in both the synaptic (bassoon-overlapping fraction) and extrasynaptic (bassoon-non-overlapping fraction) populations. Interestingly, no significant increase in the density or size of surface N-cadherin particles was observed in the NMDA-treated group (data not shown); the former

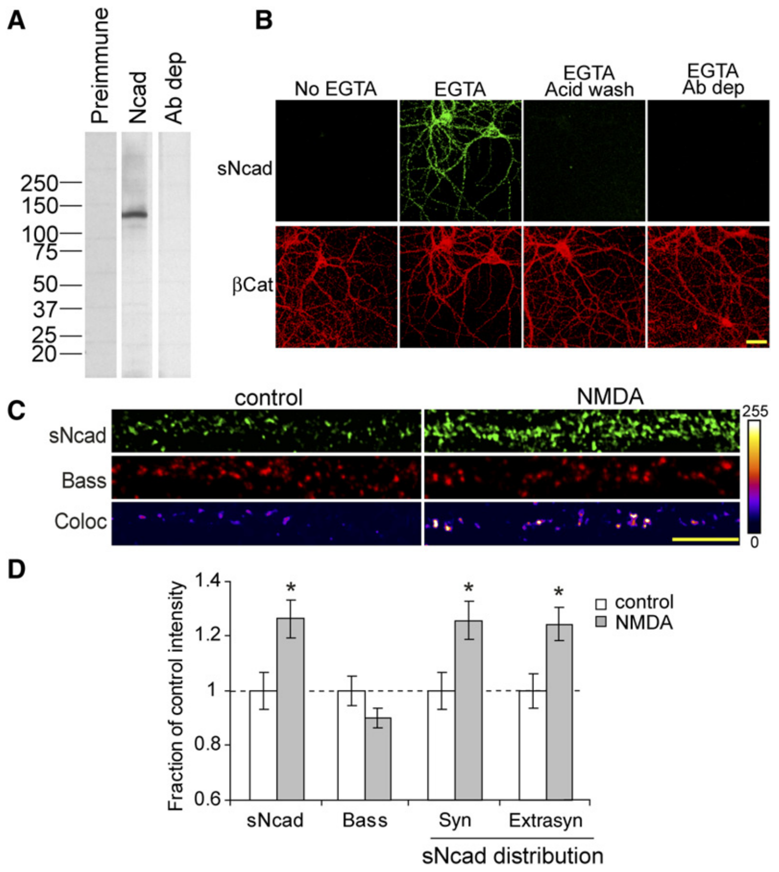

Figure 2. NMDAR Activity Stabilizes Surface N-Cadherin

(A) Specificity of the N-cadherin antibody. Homogenates of adult rat cortex were resolved by a 5%–20% gradient gel and blotted with preimmune sera (lane 1 from left), an affinity-purified N-cadherin antibody (lane 2), or an antibody-depleted (Ab dep) control (lane 3).

(B) N-cadherin surface antibody recognized the surface population of N-cadherin in the presence of the calcium chelator EGTA, but not following an acid wash or when treated with an antibody-depleted solution. Representative immunofluorescence images of neurons labeled with surface N-cadherin (sNcad, green) and β-catenin (βCat, red) (detected following permeabilization) with or without EGTA treatment are shown.

(C) NMDA treatment caused an increase in the intensity of surface N-cadherin puncta. Surface N-cadherin was labeled with the antibody prior to permeabilization (green), and a presynaptic marker, bassoon (red), was labeled after the permeabilization. Colocalized particles are shown in the lower panels. Color lookup table on the right indicates the fluorescence intensity of the colocalization on an 8-bit scale.

(D) Summary graph indicates that N-cadherin particles exhibited increased intensity in the NMDA-treated samples at both synaptic and extrasynaptic sites (mean ± SEM; control, n = 36; NMDA, n = 39 dendrites from four experiments; *$p < 0.05$). Scale bars, 10 μm.

suggests that no new N-cadherin clusters were formed, and the latter suggests that there was no expansion of preexisting N-cadherin clusters. Note that pretreatment with a protein synthesis inhibitor, anisomycin (40 μM), did not alter the effects of NMDA (data not shown), indicating that the changes observed in the NMDA-treated neurons are protein synthesis-independent. Together with the surface biotinylation experiments, these data suggest that NMDA treatment stabilizes a preexisting population of surface N-cadherin present at both synaptic and extrasynaptic sites.

The Cytoplasmic Domain of N-Cadherin Contains Multiple Motifs That Positively and Negatively Regulate Its Endocytosis

The endocytosis of N-cadherin occurs constitutively and is regulated by NMDAR activity, which suggests regulation by intracellular interactions and signaling. We thus examined whether endocytosis signals reside in the cytoplasmic domain of N-cadherin. We constructed chimeric molecules comprising the human interleukin-2 α subunit (Tac) and different subdomains of N-cadherin cytoplasmic domain (Figure 3A). These chimera constructs were tested for their ability to interact with an established N-cadherin binding partner, β-catenin (Ozawa et al., 1990). The C3 subdomain of N-cadherin was found to interact with β-catenin as previously described (Figure 3B, Ozawa et al., 1990). However, a small amount of β-catenin protein could also be immunoprecipitated by the C2 subdomain, suggesting a potential low-affinity β-catenin binding site in the C2 subdomain of N-cadherin.

We next performed antibody live-labeling assays using COS-7 cells transfected with the different chimeric proteins to determine which N-cadherin subdomains control endocytosis. We assessed the internalization of the chimeric protein using an anti-Tac antibody; two secondary antibodies were used to recognize the surface and internal population of Tac proteins. Control experiments shown in Figure 3C were performed to test the reliability of this dual-labeling technique. Following an acid wash step (see Experimental Procedures), the surface antibody signal was undetectable, whereas the internal antibody signal was absent if the incubation temperature was lowered to 4°C, a temperature prohibitive for endocytosis. To control for potential differences in the levels of surface expression among the chimeric constructs, we randomly sampled ~200–300 cells per experiment and the median value of the surface fluorescence intensity was computed for each construct. We counted the number of transfected cells containing internalized puncta and expressed the data relative to the Tac-alone control group (n = 100 cells per condition per experiment) (Figure 3D). Three

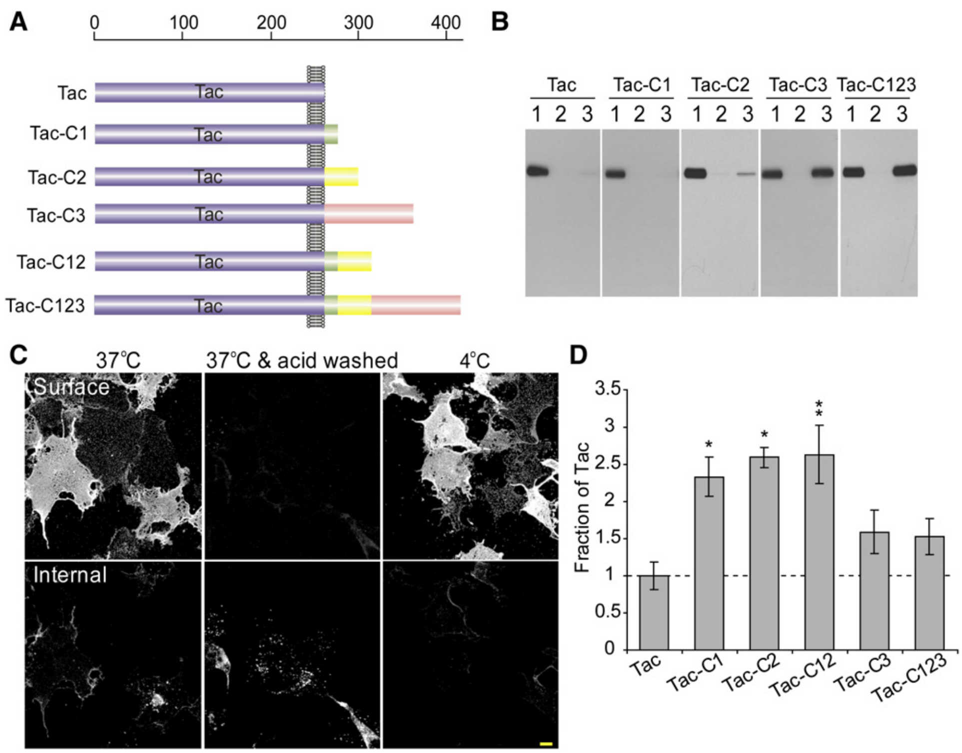

Figure 3. The Cytoplasmic Domain of N-Cadherin Contains Multiple Endocytosis Motifs

(A) Diagram of the Tac-N-cadherin chimera constructs. The cytoplasmic domain of N-cadherin is divided into three parts containing the following: C1 (green), a putative di-leucine endocytosis motif; C2 (yellow), a PEST sequence; and C3 (pink), a β-catenin binding site and a putative tyrosine-based endocytosis motif.

(B) β-catenin binds to the C3-containing Tac chimera proteins. Tac chimera proteins were immunoprecipitated from the transfected COS-7 cell lysate and blotted for β-catenin (lane 1: 5% lysate loaded; lane 2: IgG control IP; lane 3: anti-Tac Ab IP).

(C) Endocytosis assay of Tac chimera constructs in COS-7 cells. Dual-color labeling of surface and internalized signals was converted to grayscale for presentation. Scale bar, 10 μm.

(D) Summary graph of N-cadherin fragments containing β-catenin binding sites, which exhibited decreased internalization efficiency. n = 5 experiments (mean ± SEM, *p < 0.01, **p < 0.05 relative to Tac).

interesting results were observed. First, the cytoplasmic region of N-cadherin contains more than one endocytosis motif (in regions C1 and C2; Figure 3D). Moreover, there is no synergistic or additive effect when more than one endocytosis motif is present: comparable levels of endocytosis were observed when C1 or C2 was expressed versus the combination of C1 and C2. Second, the β-catenin binding domain (C3) suppresses the efficiency of endocytosis (C12 versus C123), suggesting that a negative regulatory element resides in the C3 subdomain. Lastly, the presence of C3 was dominant over C1 and C2, suggesting that the physical association of β-catenin with N-cadherin exerts potent control over N-cadherin endocytosis.

NMDAR Activity and β-Catenin

An earlier study showed that depolarization resulted in an NMDAR-dependent redistribution of β-catenin from dendritic shafts to spines in cultured hippocampal neurons (Murase et al., 2002). We examined whether direct stimulation with NMDA results in a similar redistribution. Using an EGFP-β-catenin fusion protein we performed time-lapse imaging experiments monitoring EGFP-β-catenin localization in dendrites 10 min before and 1 hr after a 3 min, 20 μM NMDA treatment (Figure 4A). We observed a gradual and persistent increase of EGFP-β-catenin in spines after NMDA application (Figure 4A, left column). Preincubation of neurons with the NMDAR antagonist APV (100 μM), however, prevented the increased localization of EGFP-β-catenin in spines (Figure 4A, middle column). Note that NMDA treatment did not alter the localization of EGFP alone (Figure 4A, right column). A persistent, NMDAR-dependent increase in the spine β-catenin signal was also observed upon the addition of bicuculline, and this increase was abolished in the presence of APV (Figure S4). Together, these results indicate that β-catenin responds to NMDAR activity by moving into dendritic spines.

What kind of dynamic changes underlie the redistribution of EGFP-β-catenin into spines? We performed fluorescence recovery after photobleaching (FRAP) experiments to monitor the entry rate of EGFP-β-catenin before and after NMDA treatment (Figure 5). In the control

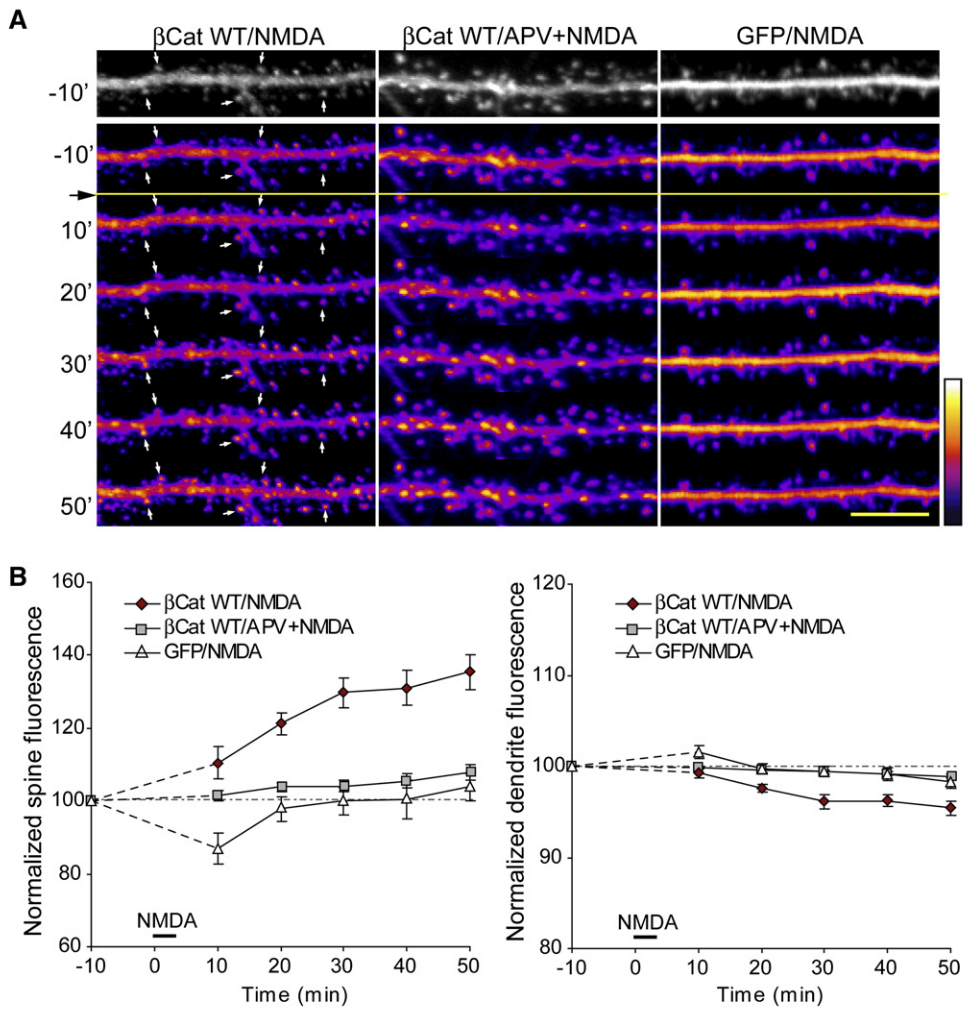

Figure 4. NMDA Application Causes a Redistribution of β-Catenin into Spines

(A) Time-lapse images of dendrites from neurons expressing either WT β-catenin (NMDA and APV+NMDA groups) or GFP as a control (GFP/NMDA). The black arrow and the yellow line indicate NMDA addition (20 μM for 3 min). White arrows indicate spines where β-catenin increased signal intensity, represented by the color lookup table on the right. Scale bar, 10 μm.

(B) Summary graphs showing the normalized spine (left) and dendritic (right) fluorescence before and after NMDA treatment, expressed as a percent of baseline fluorescence (mean ± SEM; control n = 32; βCat WT/NMDA, n = 28; βCat WT/APV+NMDA, n = 27 dendrites from four experiments). Dashed lines between −10 and 10 min time points indicate a discontinuity in image acquisition due to solution exchange. Statistical significance was assessed by ANOVA with Tukey-Kramer's post hoc test ($p < 0.05$).

group (mock treated), the time constants before and after the solution exchange were not significantly different (τ = 3.4 ± 0.4 s before and 3.5 ± 0.5 s after perfusion, respectively, Figures 5B–5E). NMDA-treated neurons, however, showed a significantly reduced time constant after NMDA exposure (τ = 3.4 ± 0.4 s before NMDA and 2.6 ± 0.3 s after NMDA), indicating an increase in the entry rate after stimulation. The general trend of fluorescence recovery agrees with a simple diffusion model in spines (Svoboda et al., 1996). We estimated the diffusion coefficients (D) to describe the speed of β-catenin diffusing into the spine before and after the NMDA treatment (D = 0.27 ± 0.02 $\mu m^2/s$ before NMDA and 0.43 ± 0.08 $\mu m^2/s$ after NMDA; see Supplemental Experimental Procedures), the results of which suggested an increase in the rate of β-catenin diffusion into spines after NMDA treatment.

Since NMDAR activation induced a persistent redistribution of β-catenin into spines (Figure 4), we reasoned there might be a stabilizing factor in the spine. To address this issue, we next performed fluorescence loss in photobleaching (FLIP) experiments to measure the immobile β-catenin fraction before and 1 hr after NMDA application. The dendritic shaft underneath the spine was bleached every 2 s, and one image was taken immediately after each bleaching episode (Figure 6A). Under control conditions, most of the EGFP-β-catenin in the spine moved into the bleached dendritic shaft (soluble/mobile fraction), and a smaller fraction remained in the spine (immobile

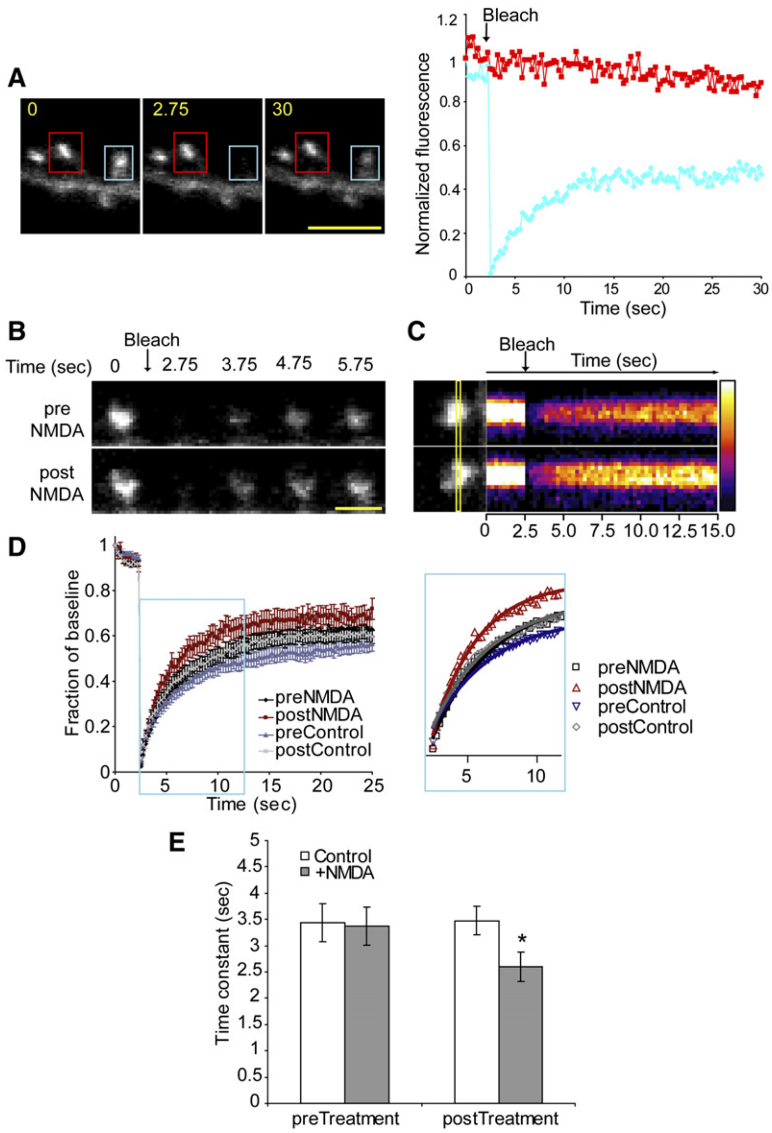

Figure 5. NMDA Treatment Accelerates β-Catenin Movement into Spines

(A) Representative FRAP experiment showing EGFP-β-catenin moving into dendritic spines. The blue box represents the area of photobleaching, and the red box represents the nearby area that was not bleached. Time stamps represent seconds. Graph shows the normalized (to the first time point of baseline) fluorescence intensity corresponding to the signals within the two colored boxes. Scale bar, 5 μm.

(B) Representative time series of a FRAP experiment before and after NMDA treatment. Scale bar, 1 μm.

(C) Kymograph showing the GFP intensity profile over time, taken from the line scan in the center of the spine head, as marked by the yellow box. Signal intensity was pseudocolored; color lookup table is shown. NMDA increased the recovery rate of the EGFP-β-catenin signal following photobleaching.

(D) Summary graph of FRAP experiments (mean ± SEM; NMDA, n = 13; Control, n = 23 cells from three experiments). All raw data were fit with a single exponential decay curve and the fit is represented by the blue box.

(E) Summary graph for time constants (mean ± SEM). NMDA treatment led to a significantly faster recovery (*$p < 0.05$).

fraction), presumably owing to association with a protein or structural element. NMDAR activation significantly increased the immobile β-catenin fraction (16.5% ± 0.02% versus 20.9% ± 0.02% for pre- and post-NMDA groups, $p < 0.05$, Figures 6A–6C). This result indicates that NMDAR activity enhances the sequestration of β-catenin in spines, presumably by enhancing its interaction with one or more spine proteins. To test whether N-cadherin is the β-catenin-interacting partner in spines after simulation, we performed immunoprecipitation assays 1 hr after NMDA treatment (Figures 6D and 6E). We observed an ~20% increase in the amount of β-catenin coimmunoprecipitated with N-cadherin in NMDA-treated neurons. In addition, we performed a crude synaptosome preparation to measure whether there is a concomitant increase in the amount of both β-catenin and N-cadherin in the synaptic fraction (Figures 6F and 6G). Indeed, an ~40% increase in the signal intensity for both β-catenin and N-cadherin was observed in the synaptic fraction. Taken together with the immunoprecipitation results, these data suggest that enhanced N-cadherin/β-catenin associations following NMDA stimulation stabilize β-catenin in spines.

Tyrosine Phosphorylation of β-Catenin Regulates NMDA-Dependent N-Cadherin Endocytosis

In vitro experiments have shown that the tyrosine phosphorylation of β-catenin reduces its binding affinity with N-cadherin (Roura et al., 1999). Does tyrosine phosphorylation of β-catenin play a role in the NMDA-dependent regulation of N-cadherin endocytosis? To address this possibility, we immunoprecipitated β-catenin protein from lysates prepared from either NMDA-treated or untreated neurons and then conducted immunoblotting with an

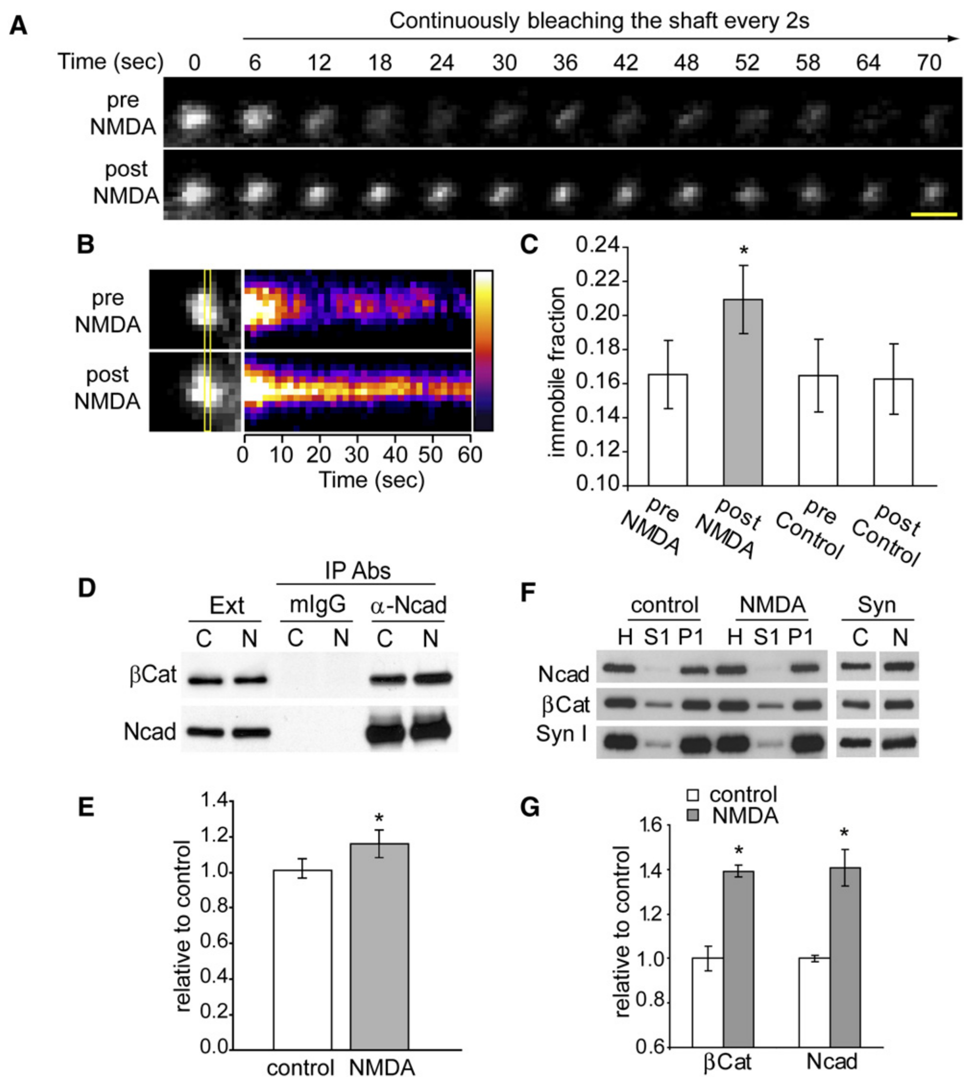

Figure 6. β-Catenin Is Retained in Spines upon Stimulation

(A) Monitoring the exit of EGFP-β-catenin from the spine while the underlying shaft area was repetitively bleached every 2 s. A spine image was taken immediately after the bleaching. NMDA treatment significantly reduced the exit rate of EGFP-β-catenin; bleaching of the post-NMDA spines was performed 1 hr after treatment. Scale bar, 1 μm.

(B) Kymograph showing the amount of EGFP-β-catenin remaining in the spine by the one-pixel line scan in the center of the spine head, as marked by the yellow box. Colorized signals represent fluorescence intensity. Less fluorescence was lost after NMDA treatment.

(C) Summary graph of the immobile fraction across the treatments (mean ± SEM, *$p < 0.05$; NMDA, n = 29; Control, n = 24 spines from five experiments).

(D) Coimmunoprecipitation of β-catenin and N-cadherin from hippocampal lysates. Probed proteins are indicated at left.

(E) Summary graph (mean ± SEM, n = 5, *$p < 0.05$) shows the relative ratio of β-catenin to N-cadherin. NMDA modestly, but significantly, enhanced the immunoprecipitation of β-catenin by N-cadherin.

(F) Representative blot of β-catenin and N-cadherin proteins in synaptosomal fraction with or without NMDA treatment (N and C, respectively). Equal amount of homogenate (H), low-speed supernatant (S1), low-speed pellet (P1), and crude synaptosome pellet (SYN) was loaded.

(G) Summary graph (mean ± SEM, n = 4, *$p < 0.05$ relative to control).

anti-phosphotyrosine specific antibody. We found there was a decrease (~20%) in the amount of tyrosine phosphorylated β-catenin in the NMDA-treated neurons (Figure 7A), consistent with an enhanced interaction between N-cadherin and β-catenin. To assess the consequence of this interaction, we examined surface expression of N-cadherin in neurons overexpressing a mutant form of β-catenin, Y654F, which exhibits enhanced association with N-cadherin (Roura et al., 1999). As predicted, Y654F expression enhanced the surface population of N-cadherin, resulting in an ~2-fold increase in both size and intensity of surface N-cadherin puncta (Figure 7B).

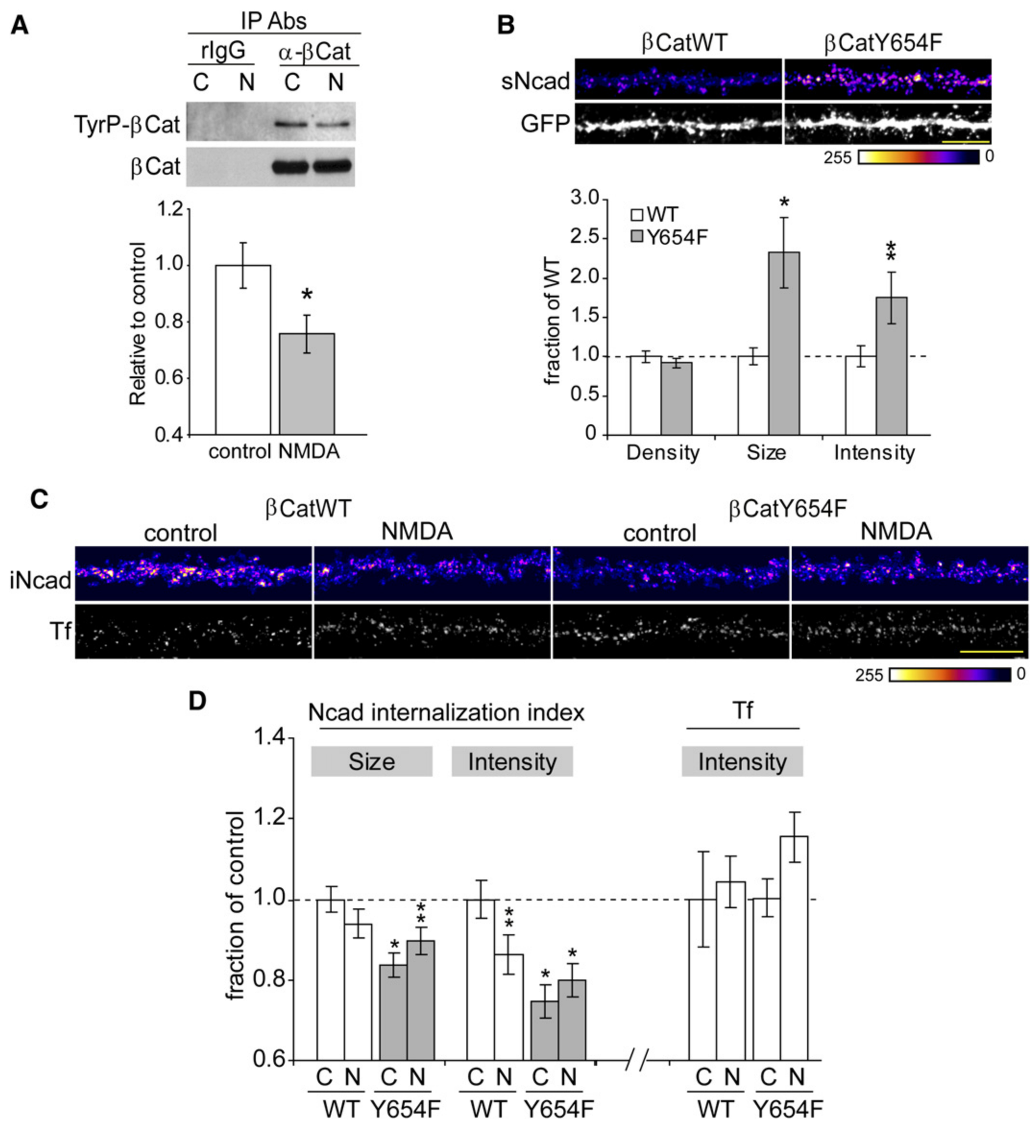

Figure 7. Tyrosine Phosphorylation of β-Catenin Regulates the NMDA-Dependent N-Cadherin Internalization

(A) The level of tyrosine phosphorylated β-catenin in control or NMDA-treated lystates. Summary graph (mean ± SEM, n = 4, *p < 0.05 relative to control) shows a decreased level of tyrosine phosphorylated β-catenin in the NMDA-treated neurons.

(B) Representative images of surface N-cadherin-labeled dendrites expressing EGFP-β-catenin proteins. Cells were incubated with the N-cadherin surface antibody on ice for 30 min as described in the Experimental Procedures. Colorized images show that the surface N-cadherin (sNcad) signals increase significantly in the β-catenin Y654F mutant overexpressing cell. Summary graph below indicates that the N-cadherin particles increased in size and intensity in the Y654F neurons (mean ± SEM, *p < 0.05, **p < 0.005 relative to WT; βCatWT, n = 20; βCatY654F = 30 from three experiments). Scale bar, 10 μm.

(C) Pseudocolored images represent the mean pixel intensity of the internalized N-cadherin (iNcad) in dendrites expressing β-catenin EGFP-WT or EGFP-Y654F. A dramatic decrease in the amount of iNcad was observed in the βCatWT/NMDA neurons when compared with that of the βCatWT/control neurons, whereas neurons expressing Y654F-EGFP did not exhibit this decrease. Overexpression of either WT βCat orY654F did not interfere with the constitutive endocytosis of the transferrin (Tf). Scale bar, 10 μm.

(D) Summary graph demonstrates a significant drop in the mean puncta size and intensity in the Y654F neurons. In the NMDA-treated (N) Y654F neurons, there was a decrease of iNcad intensity when compared with the untreated (C) Y654F neurons (mean ± SEM, **p < 0.05, *p < 0.005 relative to WT; Ncad internalization index: WT/C, n = 41; WT/N, n = 40; Y654F/C, n = 45; Y654F/N, n = 41, Tf: WT/C, n = 29; WT/N, n = 30; Y654F/C, n = 30; Y654F/N, n = 30, cells from three experiments).

To examine whether this enhanced surface expression of N-cadherin was due to altered endocytic trafficking, cultured hippocampal neurons expressing either WT or Y654F β-catenin were subjected to our N-cadherin antibody live-labeling technique for a measurement of N-cadherin endocytosis (see Experimental Procedures). In control experiments, we validated our dual-labeling procedure with the same acid wash protocol described in Figure 3C and the Experimental Procedures (Figure S5). In the Y654F-expressing neurons, both the size and intensity of the internalized N-cadherin puncta were dramatically reduced when compared with the puncta in WT-expressing neurons (Figures 7C and 7D). Most importantly, the NMDA-elicited reduction of N-cadherin endocytosis was abolished in the Y654F neurons (compare the two gray intensity columns in Figure 7D), suggesting that the tyrosine residue 654 is responsible for the effects of NMDAR activity. We observed that the endocytosis of a control protein, transferrin (Tf), was unaffected by the β-catenin mutant. Taken together, these results indicate that the tyrosine phosphorylation of β-catenin regulates the endocytosis of N-cadherin in an NMDAR activity-dependent manner.

Prolonged Stability of Surface N-Cadherin Blocks NMDAR-Dependent LTD

Given that NMDA treatment delays N-cadherin endocytosis, we predicted that the removal of such regulation would affect NMDAR-related synaptic plasticity. Addition of NMDA to cultured hippocampal neurons has been reported to produce a chemical long-term depression (chemLTD), which manifests as a decrease in the frequency, and subtle reduction of the amplitude, of mEPSCs (Figure S3, e.g., Beattie et al., 2000). To monitor NMDAR-dependent LTD, we recorded mEPSCs from cultured hippocampal neurons. After a 5 min baseline recording, neurons were treated with 20 μM NMDA for 3 min, and then 100 μM APV was added to inactivate the NMDAR for another 5 min (NMDA group in Figures S3A and S3B). As expected, we observed a decrease in mEPSC frequency in the NMDA-treated neurons but not in the vehicle-treated neurons (Mock group) (Figure S3). Next, we recorded mEPSCs from neurons expressing either WT or Y654F β-catenin proteins using the same NMDA treatment protocol. Note that we observed an elevated mEPSC frequency in Y654F neurons when compared with that of WT neurons (Figures 8A and 8B) (1.03 ± 0.07 Hz and 1.28 ± 0.05 Hz for WT and Y654F, respectively), similar to a previous report (Murase et al., 2002). As previously observed, NMDA treatment resulted in a reduction in mEPSC frequency in WT-expressing neurons (71.1% ± 7.5% relative to baseline, Figures 8C and 8D) and a slight and not statistically significant decrease in amplitude (14.4% ± 5.4% relative to baseline), suggesting that overexpression of WT β-catenin does not interfere with this form of LTD. In contrast, neurons expressing the Y654F β-catenin mutant did not exhibit an NMDA-induced decrease in mEPSC frequency (107.1% ± 6.2% relative to baseline, Figures 8C and 8D), indicating that this form of NMDA-dependent plasticity is abolished in this mutant.

DISCUSSION

Here we demonstrate that the endocytosis of N-cadherin is highly regulated and coupled to NMDAR-dependent neuronal activity. NMDA treatment causes a delay in the endocytosis of N-cadherin and the accumulation of surface N-cadherin molecules. Several lines of evidence suggest that β-catenin is important in this process. Binding of β-catenin negatively regulates the internalization of N-cadherin in both heterologous cells and neurons. In addition, NMDAR activity elicits changes in β-catenin biochemical and dynamic properties. A decreased level of tyrosine phosphorylated β-catenin and strengthened N-cadherin/β-catenin association was detected in NMDA-treated neurons. The rate of β-catenin movement into spines increased after NMDA application. Prolonged stabilization of N-cadherin at the surface was accompanied by a blockade in the reduction of mEPSC frequency after NMDA treatment. These results indicate that the regulation of N-cadherin endocytosis is one mechanism by which N-cadherin exerts its effects on synaptic function and plasticity.

Constitutive and Activity-Regulated Endocytosis of N-Cadherin in Neurons

We have conducted a detailed analysis of N-cadherin internalization from the neuronal plasma membrane. A large fraction (~43%) of surface N-cadherin protein undergoes constitutive endocytosis. Moreover, the internalized population of N-cadherin is rapidly recycled back to the surface with a time constant of ~10 min, almost three times faster than the rate of internalization, suggesting there is only a small fraction of N-cadherin present in the recycling compartment at any given time. Unlike surface N-cadherin endocytosis, the rate of recycling is not affected by NMDAR activation. Our observation that NMDA slows N-cadherin endocytosis is strikingly different from its effects on the endocytosis of AMPAR, as NMDA accelerates AMPAR's internalization (Figure S3, e.g., Beattie et al., 2000; Ehlers, 2000; Lin et al., 2000; Man et al., 2000). The accelerated internalization of AMPAR upon agonist stimulation has been proposed as a mechanism to desensitize the response to neurotransmitter (Carroll et al., 2001). In the case of NMDA-regulated N-cadherin endocytosis, NMDA application causes an accumulation of surface N-cadherin, suggesting a stabilization of synaptic structures while AMPAR is being internalized. This hypothesis is consistent with the observation that spine motility is dramatically reduced upon NMDA application (Brunig et al., 2004; Fischer et al., 2000). We propose that internalization of AMPAR associated with agonist treatment prompts a significant reorganization of the synaptic space: the opposing stability of N-cadherin may be required to counteract the destabilizing influence of receptor internalization, creating a structural memory of the synapse.

β-Catenin and Activity-Regulated N-Cadherin Endocytosis

Previous studies suggested that the tyrosine phosphorylation of β-catenin decreases its binding affinity with cadherin (Roura et al., 1999), and the cadherin zipper structure becomes disorganized in the absence of

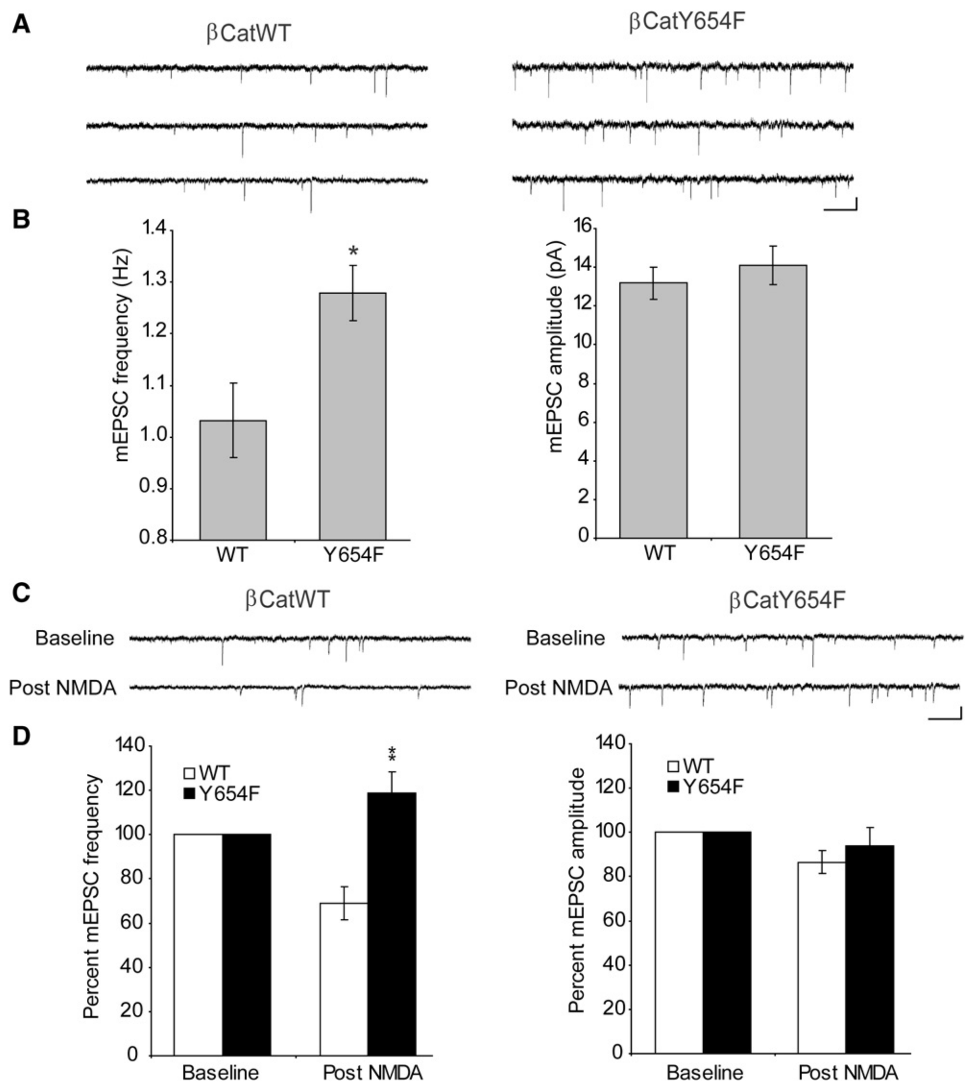

Figure 8. Mutation of a β-Catenin Tyrosine Residue Blocks NMDA-Mediated LTD in Cultured Hippocampal Neurons

(A) Sample traces recorded from neurons expressing either β-catenin WT or Y654F. Scale bar, 10 pA, 500 ms.

(B) Mean mEPSC frequency and amplitude in WT (n = 13 cells) or Y654F (n = 13 cells) neurons. $^*p < 0.01$.

(C) Sample traces from β-catenin WT- or Y654F-expressing neurons taken either 2–4 min before (baseline) or 4–6 min after NMDA application. There was no decrease in mEPSC frequency in the NMDA-treated Y654F neurons. A small increase in frequency was observed in Y654F-expressing neurons, which was not statistically significant.

(D) Summary data. n = 8, n = 9 cells for WT- and Y654F-expressing neurons, respectively. $^{**}p < 0.05$ relative to WT. Scale bar, 10 pA, 500 ms.

a β-catenin binding (Huber et al., 2001). Our data indicate that β-catenin plays a negative role in regulating the endocytosis of N-cadherin in both heterologous and neuronal cells (Figure 3 and Figure 7). In our earlier work we observed an increase in spine localization of β-catenin upon NMDAR activation (Murase et al., 2002), and we have found that this redistribution is due to an increased rate of β-catenin entry into dendritic spines (Figure 5). In addition, there was a decrease in the amount of tyrosine phosphorylated β-catenin (Figure 7), an increased N-cadherin/β-catenin association, and an increased concentration of β-catenin in spines (Figure 4, Figure 5, and Figure 6). These results indicate that NMDAR activity reduces the tyrosine phosphorylation of β-catenin and leads to an increased interaction between β-catenin and N-cadherin. It remains to be determined whether this regulation occurs via control of a tyrosine kinase or phosphatase. Nevertheless, it is worth noting that β-catenin is a direct substrate of LAR receptor tyrosine phosphatase; overexpression of a dominant-negative LAR blocks dendritic targeting of β-catenin (Dunah et al., 2005; Kypta et al., 1996). LAR interacts with the AMPAR complex through liprin at the synapse, suggesting that this tyrosine phosphatase is a candidate for the activity-regulated tyrosine dephosphorylaton of β-catenin (Dunah et al., 2005; Wyszynski et al., 2002).

A proteomic analysis of proteins associated with the NMDAR complex revealed both N-cadherin and β-catenin, suggesting a direct or indirect association of these molecules with NMDAR (Husi et al., 2000). Our results support a biochemical interaction documenting a reciprocal regulation between NMDAR activity and N-cadherin endocytosis. On one hand, upon NMDAR stimulation, the endocytosis of N-cadherin is delayed, resulting in an accumulation of surface N-cadherin (Figure 1 and Figure 2). On the other hand, prolonged stabilization of surface N-cadherin results in a blockade of the NMDAR-dependent form of LTD (Figure 8). Furthermore, N-cadherin and β-catenin are found in the AMPAR immunoprecipitates, suggesting the importance of cadherin/catenin adhesion complex in regulating AMPAR function (Dunah et al., 2005; Nuriya and Huganir, 2006).

Functional Implications of N-Cadherin Endocytosis in Synaptic Plasticity

In spines, the endocytic zones reside in specialized areas lateral to the postsynaptic density (PSD) (Blanpied et al., 2002; Racz et al., 2004). It has been hypothesized that mobile proteins must uncouple from the PSD and move laterally prior to endocytosis (reviewed by Triller and Choquet, 2005). Moreover, the diffusion constant of glutamate receptor within the synapse is ~5-fold lower than that in the extra-synaptic membrane, suggesting that high concentrations of adhesion molecules in the synaptic compartment can interfere with the diffusion of glutamate receptors (Tardin et al., 2003). Interestingly, N-cadherin has been observed to localize at the outer rim of the synaptic contacts (Beesley et al., 1995; Fannon and Colman, 1996; Phillips et al., 2001; Uchida et al., 1996), either forming an enclosed circle around the PSD (Fannon and Colman, 1996) or concentrating at the edges of the PSD (Spacek and Harris, 1998; Uchida et al., 1996). Because N-cadherin borders the synaptic region, its abundance will likely set limits on the diffusion of synaptic molecules into and out of the synapse. Interestingly, NMDA treatment has been observed to decrease the association of another synaptic protein, A-kinase-anchoring protein (AKAP), with AMPAR, enabling its internalization (Gorski et al., 2005). AKAP79/150 has also been proposed to compete with β-catenin for N-cadherin interactions. This idea fits well with our data: NMDA treatment promotes the concentration of β-catenin in spines and the stabilization of surface N-cadherin and the synaptic scaffold during the period of AMPAR endocytosis.

The activity-regulated AMPAR trafficking at postsynaptic sites underlies some forms of plasticity, such as LTP or LTD (Malenka, 2003). NMDA treatment is known to induce massive internalization of AMPAR and this been proposed to underlie NMDA-dependent LTD (Beattie et al., 2000; Ehlers, 2000; Lin et al., 2000; Man et al., 2000). In addition, there is no change in paired pulse facilitation in chemLTD-induced hippocampal slices, suggesting chemLTD is not triggered by a presynaptic mechanism (Lee et al., 1998). We previously demonstrated that expression of Y654F in postsynaptic cells brings about both pre- and postsynaptic changes (increased size of synapsin I, FM4-64, and PSD95 puncta) (Murase et al., 2002). We suggest that Y654F occludes the NMDA-induced LTD because the cadherin/catenin adhesion complex is already stabilized. The relative enhancement of mini frequency observed in Y654F-expressing neurons is likely due to additional presynaptic effects of Y654F expression, which are not produced by NMDA treatment.

Taken together, the data presented here suggest that synaptic adhesion molecules, usually considered static and relatively immobile, are constantly trafficked in and out of the membrane. This dynamic behavior provides flexibility for regulating adhesive forces and signaling in response to neuronal activity. Activity triggers changes in both the biochemical properties and spatial localization of intracellular signaling molecules in order to regulate the endocytosis of adhesion molecules. These data thus highlight a novel regulatory pathway that couples synaptic structural components with neuronal activity and plasticity.

EXPERIMENTAL PROCEDURES

Cultured Hippocampal Neuron and Mammalian Cell Lines

Dissociated hippocampal neurons were prepared and maintained as previously described (Aakalu et al., 2001). Briefly, hippocampi from postnatal day 0 to 2 were dissected out and dissociated by either trypsin or papain and plated at a density of 55,000–70,000 cells/cm^2 onto poly-D-lysine-coated glass-bottom Petri dishes (Mattek) or 35 mm culture dishes (Falcon). Cultures were maintained in Neurobasal A medium containing B-27 and Glutamax supplements (Invitrogen) at 37°C for 18–20 days before use. BHK and COS-7 cells (ATCC) were grown in Dulbecco's modified Eagle's medium with 10% fetal bovine serum and penicillin/streptomycin (Invitrogen).

Transient Transfection and Viral Infection

For transient transfection, COS-7 cells were plated either onto an 18 mm square coverslip in a 6-well dish for microscopy or in a 35 mm culture dish for immunoprecipitation, grown to 80%–90% confluence, then transfected with an appropriate amount of DNA mixed with lipofectAMINE (Invitrogen). Transient expression was allowed for 40 to 48 hr. For Sindbis viral infection, 16–21 days in vitro (div) neurons were infected with recombinant Sindbis virus coding for EGFP (Aakalu et al., 2001), EGFP-β-catenin WT, or Y654F transcripts (Murase et al., 2002), and proteins were allowed to express for at least 12 hr.

N-Cadherin Surface Antibody Production, Purification, and Depletion

Full-length mouse N-cadherin cDNA in a mammalian expression vector (pCXN2-Ncad) was provided by Dr. Deanna Benson. A BamHI-EcoRV fragment of the N-cadherin EC domain, aa 308–597, was cloned into the BamHI-SmaI site of pGEX5P-2 vector (GE Biosciences), and resulted in an in-frame fusion between GST and the N-cadherin fragment. The fusion protein was recovered from the insoluble fraction of the bacterial lysate by an Inclusion Solubilization Buffer (Pierce) and dialyzed into a buffer containing 25 mM Tris-HCl (pH 7.5), 150 mM NaCl, and 2 mM $CaCl_2$. A polyclonal antibody against the GST fusion protein of N-cadherin was raised using ascites fluid. Total IgG was purified using Protein G affinity chromatography (GE Biosciences) according to the manufacturer's instructions. The N-cadherin-specific

IgG was depleted by incubating the purified total IgG with the antigen fixed on PVDF membrane (BioRad). The incubation process was repeated three times until the N-cadherin signal became undetectable by immunoblotting.

DNA Constructs

Tac cDNA construct was provided by Dr. Juan S. Bonifacino. To generate fusion constructs between Tac and N-cadherin, we added a Kozak sequence in front of the start codon of N-cadherin Tac protein and moved the entire cDNA into a different expression vector, pcDNA3.1Zeo(-) (Invitrogen). All PCR-modified constructs were confirmed by DNA sequencing. Details regarding the design of PCR primers are described in Supplemental Experimental Procedures.

Immunoprecipitation and Synaptosome Preparation

For immunoprecipitation, treated and control neurons grown in 35 mm culture dishes were rinsed twice with ice-cold PBS-MC buffer (phosphate-buffered saline, 1 mM $MgCl_2$, and 0.1 mM $CaCl_2$) and lysed with 1% NP40 lysis buffer (1% NP40, 150 mM NaCl, and 50 mM Tris-HCl [pH 8.0]) containing protease inhibitor cocktail. The detergent-extracted lysates were mixed with Protein G beads (Pierce) with 5 μg of rabbit or mouse IgG (Jackson ImmunoResearch) and incubated at 4°C overnight with gentle rotation for a preclearing step. The precleared extracts were mixed with Protein G beads with 1 μg of target protein antibody or with 1 μg control IgG, and incubated at 4°C overnight with rotation. Beads were washed with lysis buffer and boiled in 5× SDS-PAGE sample buffer. The entire eluate, along with 2% of the supernatant, was loaded onto 7.5% SDS-polyacrylamide gel and transferred onto PVDF membrane (BioRad). Immunoblotting was performed with various antibodies against tags or specific proteins, and HRP-conjugated secondary antibodies (Jackson Immunoresearch) were applied prior to ECL detection (GE Biosciences). For synaptosome preparation, treated and control neurons were homogenized in 0.32 M sucrose buffer (0.32 M sucrose and 4 mM HEPES [pH 7.4]) with protease inhibitor cocktail as described earlier (Bagni et al., 2000). Films were scanned, and the sum of the pixel intensity in each lane was analyzed by ImageJ (NIH). The amount of the target protein being precipitated per lane was used as loading control for the immunoprecipitation experiments. The following antibodies were used for immunoprecipitation and blotting: rabbit anti-β-catenin (Zymed), mouse anti-Tac (Covance), mouse anti-N-cadherin (BD Transduction Lab), rabbit anti-synapsin I (Chemicon), and anti-RC20: HRPO (BD Transduction Lab). Statistical significance was assessed by the paired Student's t test unless noted otherwise.

Surface Biotinylation for Endocytosis and Recycling Assays

Cultured hippocampal neurons (13–19 div) grown in 35 mm dishes were incubated with 100 μg/ml leupeptin (and 100 μM APV for +APV samples; Sigma) for 1 hr at 37°C to block the activity of lysosomes or NMDAR. Surface proteins were prelabeled with 0.3 mg/ml of membrane-impermeable Sulfo-NHS-SS-biotin (Pierce) in PBS-MC on ice for 12 min. Unbound biotin was quenched by Tris buffer (25 mM Tris-HCl [pH 8.0], 133 mM NaCl, and 10 mM KCl) followed by 20 μM NMDA (Sigma) treatment in growth media for 3 min at 37°C. Neurons were then rinsed with fresh growth media twice and returned back to the incubator for various periods of time as indicated in Figure 1. At the end of each time point, neurons were quickly chilled down to 4°C by rinsing with ice-cold PBS-MC, and the surface biotin group was removed by incubating with 50 mM glutathione solution (50 mM reduced glutathione, 75 mM NaCl, 10 mM EDTA [pH 7.5], 1% BSA, and 0.075 N NaOH) twice for 15 min on ice. Neurons were then lysed with 1% Triton X-100/0.1% SDS/PB (20 mM $NaPO_4$ [pH 7.5 buffer] and 150 mM NaCl) including a protease inhibitor cocktail (Roche). The internalized and/or biotinylated proteins were isolated by incubating with NeutrAvidin beads (Pierce) overnight for 2 hr at 4°C. Total internalized/biotinylated proteins were separated and analyzed by SDS-PAGE followed by immunoblotting for individual proteins. The amount of protein in the lysate was used as the loading control for the biotinylation experiments. Results were fit with a single exponential growth curve as described previously with an $r^2 > 0.85$ (Ehlers, 2000). Statistical significance was determined by one-way ANOVA with Tukey-Kramer's post hoc test.

For the recycling assays, neurons were biotinylated and returned back to the 37°C incubator for 1 hr, and the remaining surface biotin groups were removed by one round of glutathione treatment. The internalized and biotinylated proteins were spared from the first stripping. Neurons were then treated with or without 20 μM NMDA for 3 min, followed by rinsing, and returned back to the incubator for variable intervals. A second round of glutathione treatment was applied immediately at the end of each time point. The disappearance of biotinylated proteins as a function of time represents the rate of recycling. Results were fitted with a single exponential decay curve with an $r^2 > 0.85$ (Ehlers, 2000).

Antibody Live-Labeling and Immunostaining

For N-cadherin antibody live-labeling, neurons were treated with or without 20 μM NMDA for 3 min in growth media at 37°C, followed by two rinses with prewarmed growth media, and conditioned growth media was added back and neurons were returned to the 37°C incubator for 1 hr. Neurons were removed from the incubator after the 1 hr incubation period and rinsed three times with ice-cold HBS/EGTA buffer (HEPES buffered saline [pH 7.4] without calcium and with 1 mM EGTA) and incubated on ice (note: there was minimal or no endocytosis when cells were incubated on ice) in the presence of N-cadherin surface antibody (1 mg/ml, 1:50 dilution in HBS/EGTA buffer) for 30 min (Figures 2B and 2C, Figure 7B, and Figure S5, right column), or incubated at 37°C for 10 min (Figure S5, left column, and Figure 7C). Neurons were rinsed three times with ice-cold PBS-MC and fixed with 4% formaldehyde/4% sucrose/PBS-MC on ice for 20 min, followed by incubating with a secondary antibody against the surface N-cadherin primary antibody for 1 hr at room temperature (RT). Cells were permeabilized with 0.1% Triton X-100/2% BSA/4% normal goat serum/PBS-MC on ice for 15 min. After extensive rinsing with PBS-MC, neurons were incubated with primary and secondary antibodies against the intracellular proteins sequentially for 1 hr each at RT. Finally, neurons were mounted in the Gold Prolonged Antifade reagent (Invitrogen) prior to imaging.

The dual-color immunofluorescence internalization assays for the transfected COS-7 cells (Figures 3C and 3D) or neurons (Figure 7C) were performed as described in Lin et al. (2000). In brief, cells were incubated with antibodies at 37°C for either 15 min (for anti-Tac antibody) or 10 min (for anti-N-cadherin antibody). Immediately after the antibody incubation period, cells were washed with ice-cold PBS-MC and fixed. After the 20 min blocking (2% BSA/4% normal goat serum/PBS-MC) period at RT, an Alexa 546 conjugated secondary antibody was added before permeabilization (surface) followed by an Alexa 488 conjugated secondary antibody incubation after the permeabilization (internal). A few sets of acid-wash control experiments (Figure 2B, Figure 3C, and Figure S5) were conducted with an additional acid wash (0.2 M acetic acid, 0.5 M NaCl) on ice for 3 min prior to the fixation (Dore et al., 1997). For the Tf internalization assays (Figure 7C), neurons were treated with or without NMDA and fed with 20 μg/ml of Tf conjugated with Alexa 568 (Invitrogen) for 10 min at 37°C followed by ice-cold PBS-MC rinsing, then processed as described above.

The following antibodies were used: rabbit anti-β-catenin (1:500, Zymed), mouse anti-bassoon (1:1000, StressGen), chicken anti-GFP (1:1000, Aves Lab), mouse anti-N-cadherin (1:50, BD Transduction Lab), mouse anti-CaMKIIα (1:1000, Chemicon), rabbit anti-MAP2 (1:500, BD Transduction Lab), goat anti-mouse Alexa 488 (1:1000), goat anti-chicken Alexa 488 (1:1000), goat anti-rabbit Alexa 546 (1:1000), and goat anti-mouse Alexa 633 (1:1000, Invitrogen). Double labeling of surface N-cadherin and bassoon was performed as described above, except that the anti-bassoon antibody was prelabeled with Alexa 647 IgG2a by Zenon technology (Invitrogen). This prelabeled anti-bassoon antibody was added after the incubation of all other secondary antibodies for GFP and surface N-cadherin for another 30 min at RT. A light fixation step (half strength of the fixation solution, 5 min at RT) was applied after the anti-bassoon incubation.

Image Acquisition and Analysis

All images were acquired with a Zeiss 510 Meta laser scanning confocal microscope with either a 40× (NA = 1.3) or a 63× (NA = 1.4) oil objective. For three-color colocalization studies, Alexa 488 was excited with the 488 nm line of an argon ion laser, and emitted light was collected between 510 and 550 nm. Alexa 546 was excited with the 546 nm laser, and emitted light was collected between 550 and 600 nm. Alexa 633 was excited with the 633 nm laser, and emitted light was collected above 600 nm. Each channel was acquired separately to ensure no bleedthrough between channels. All neurons in each experiment were imaged with the same microscopic settings. For live imaging experiments, the scope was fitted with a motorized stage (Applied Scientific Instrumentation) to track multiple imaging coordinates. Neurons were kept in a 37°C bath throughout the experiment by continuous perfusion of a warm HBS solution through a heating element (Warner Instrument) and a pump (Ismatec) with a flow rate of 1.5 or 2.3 ml/min. GFP was excited with the argon ion laser, and emitted light was collected above 510 nm. Optimal laser power was adjusted empirically to minimize photobleaching (see Figure 5A for example). For spine β-catenin redistribution experiments (Figure 4 and Figure S4), confocal stacks were acquired every 10 min with a pinhole equaling 1 Airy unit. For FRAP and FLIP experiments (Figure 5 and Figure 6, respectively), time series were collected with a single confocal slice (pinhole = 3.89 Airy units) every 250 ms (FRAP) or 2 s (FLIP) with 0.1% laser power. Photobleaching was performed with 100% laser power with five or ten iterations within a manually drawn region of interest (ROI). Care was taken when defining the bleaching ROI such that no bleaching into different dendritic compartments was observed.

For Tac internalization assays in the transfected COS-7 cells (Figures 3C and 3D), 20 random fields containing ~5–15 transfected cells of each construct were imaged with the optimal pinhole unit (1 Airy unit), and a maximal intensity z-projection was made from a ~15–25 μm stack.

All acquired images were processed by ImageJ (NIH) and Matlab (The MathWorks, Inc.) software. Detailed image analyses are described in the Supplemental Experimental Procedures.

Electrophysiology

Whole-cell recording were made from 18–21 div cultured hippocampal neurons in low-magnesium HBS buffer (Murase et al., 2002) containing 1 μM tetrodotoxin (Calbiochem) and 20 μM bicuculline (Sigma) using an Axoclamp amplifier (Axopatch 200B). Whole-cell pipette internal solution consisted of 100 mM cesium gluconate, 0.2 mM EGTA, 5 mM $MgCl_2$, 2 mM adenosine triphosphate, 0.3 mM guanosine triphosphate, and 40 mM HEPES (pH 7.2), and had resistance ranging from 2.5 to 5 MΩ. Neurons were recorded with a voltage clamp at −70mV, and series resistance with a change greater than 15% was excluded from the analysis using Synaptosoft Mini Analysis software. Baseline recordings were recorded for 5 min, and then 20 μM NMDA was applied into the bath for 3 min followed by the addition of 100 μM APV; recording continued for another 5 min. For Sindbis viral-infected neurons, GFP neurons were visualized under a Nikon Diaphot 300 fluorescent microscope with a 20× air objective (NA = 0.75).

Supplemental Data

The Supplemental Data for this article can be found online at http://www.neuron.org/cgi/content/full/54/5/771/DC1/.

ACKNOWLEDGMENTS

We thank H. Weld and L. Chen for making beautiful cultured hippocampal neurons; and S.A. Kim, M.A. Sutton, D. Dieterich, and Y.J. Yoon for critical review of the manuscript. This work was supported by NIH (E.M.S.). E.M.S. is an investigator of the Howard Hughes Medical Institute.

Received: November 2, 2006
Revised: March 23, 2007
Accepted: May 9, 2007
Published: June 6, 2007

REFERENCES

Aakalu, G., Smith, W.B., Nguyen, N., Jiang, C., and Schuman, E.M. (2001). Dynamic visualization of local protein synthesis in hippocampal neurons. Neuron *30*, 489–502.

Abe, K., Chisaka, O., Van Roy, F., and Takeichi, M. (2004). Stability of dendritic spines and synaptic contacts is controlled by alpha N-catenin. Nat. Neurosci. *7*, 357–363.

Bagni, C., Mannucci, L., Dotti, C.G., and Amaldi, F. (2000). Chemical stimulation of synaptosomes modulates alpha -Ca2+/calmodulin-dependent protein kinase II mRNA association to polysomes. J. Neurosci. *20*, RC76.

Bailey, C.H., Chen, M., Keller, F., and Kandel, E.R. (1992). Serotonin-mediated endocytosis of apCAM: an early step of learning-related synaptic growth in Aplysia. Science *256*, 645–649.

Beattie, E.C., Carroll, R.C., Yu, X., Morishita, W., Yasuda, H., von Zastrow, M., and Malenka, R.C. (2000). Regulation of AMPA receptor endocytosis by a signaling mechanism shared with LTD. Nat. Neurosci. *3*, 1291–1300.

Beesley, P.W., Mummery, R., and Tibaldi, J. (1995). N-cadherin is a major glycoprotein component of isolated rat forebrain postsynaptic densities. J. Neurochem. *64*, 2288–2294.

Benson, D.L., and Tanaka, H. (1998). N-cadherin redistribution during synaptogenesis in hippocampal neurons. J. Neurosci. *18*, 6892–6904.

Bienz, M. (2005). beta-Catenin: a pivot between cell adhesion and Wnt signalling. Curr. Biol. *15*, R64–R67.

Blanpied, T.A., Scott, D.B., and Ehlers, M.D. (2002). Dynamics and regulation of clathrin coats at specialized endocytic zones of dendrites and spines. Neuron *36*, 435–449.

Bozdagi, O., Shan, W., Tanaka, H., Benson, D.L., and Huntley, G.W. (2000). Increasing numbers of synaptic puncta during late-phase LTP: N-cadherin is synthesized, recruited to synaptic sites, and required for potentiation. Neuron *28*, 245–259.

Bozdagi, O., Valcin, M., Poskanzer, K., Tanaka, H., and Benson, D.L. (2004). Temporally distinct demands for classic cadherins in synapse formation and maturation. Mol. Cell. Neurosci. *27*, 509–521.

Brunig, I., Kaech, S., Brinkhaus, H., Oertner, T.G., and Matus, A. (2004). Influx of extracellular calcium regulates actin-dependent morphological plasticity in dendritic spines. Neuropharmacology *47*, 669–676.

Bryant, D.M., and Stow, J.L. (2004). The ins and outs of E-cadherin trafficking. Trends Cell Biol. *14*, 427–434.

Carroll, R.C., Beattie, E.C., von Zastrow, M., and Malenka, R.C. (2001). Role of AMPA receptor endocytosis in synaptic plasticity. Nat. Rev. Neurosci. *2*, 315–324.

Dore, S., Kar, S., and Quirion, R. (1997). Presence and differential internalization of two distinct insulin-like growth factor receptors in rat hippocampal neurons. Neuroscience *78*, 373–383.

Dunah, A.W., Hueske, E., Wyszynski, M., Hoogenraad, C.C., Jaworski, J., Pak, D.T., Simonetta, A., Liu, G., and Sheng, M. (2005). LAR receptor protein tyrosine phosphatases in the development and maintenance of excitatory synapses. Nat. Neurosci. *8*, 458–467.

Ehlers, M.D. (2000). Reinsertion or degradation of AMPA receptors determined by activity-dependent endocytic sorting. Neuron *28*, 511–525.

Fannon, A.M., and Colman, D.R. (1996). A model for central synaptic junctional complex formation based on the differential adhesive specificities of the cadherins. Neuron *17*, 423–434.

Fischer, M., Kaech, S., Wagner, U., Brinkhaus, H., and Matus, A. (2000). Glutamate receptors regulate actin-based plasticity in dendritic spines. Nat. Neurosci. *3*, 887–894.

Gorski, J.A., Gomez, L.L., Scott, J.D., and Dell'Acqua, M.L. (2005). Association of an A-kinase-anchoring protein signaling scaffold with cadherin adhesion molecules in neurons and epithelial cells. Mol. Biol. Cell *16*, 3574–3590.

Huber, A.H., Stewart, D.B., Laurents, D.V., Nelson, W.J., and Weis, W.I. (2001). The cadherin cytoplasmic domain is unstructured in the absence of beta-catenin. A possible mechanism for regulating cadherin turnover. J. Biol. Chem. *276*, 12301–12309.

Husi, H., Ward, M.A., Choudhary, J.S., Blackstock, W.P., and Grant, S.G. (2000). Proteomic analysis of NMDA receptor-adhesion protein signaling complexes. Nat. Neurosci. *3*, 661–669.

Kosik, K.S., Donahue, C.P., Israely, I., Liu, X., and Ochiishi, T. (2005). Delta-catenin at the synaptic-adherens junction. Trends Cell Biol. *15*, 172–178.

Kypta, R.M., Su, H., and Reichardt, L.F. (1996). Association between a transmembrane protein tyrosine phosphatase and the cadherin-catenin complex. J. Cell Biol. *134*, 1519–1529.

Le, T.L., Yap, A.S., and Stow, J.L. (1999). Recycling of E-cadherin: a potential mechanism for regulating cadherin dynamics. J. Cell Biol. *146*, 219–232.

Lee, H.K., Kameyama, K., Huganir, R.L., and Bear, M.F. (1998). NMDA induces long-term synaptic depression and dephosphorylation of the GluR1 subunit of AMPA receptors in hippocampus. Neuron *21*, 1151–1162.

Lin, J.W., Ju, W., Foster, K., Lee, S.H., Ahmadian, G., Wyszynski, M., Wang, Y.T., and Sheng, M. (2000). Distinct molecular mechanisms and divergent endocytotic pathways of AMPA receptor internalization. Nat. Neurosci. *3*, 1282–1290.

Malenka, R.C. (2003). Synaptic plasticity and AMPA receptor trafficking. Ann. N Y Acad. Sci. *1003*, 1–11.

Man, H.Y., Lin, J.W., Ju, W.H., Ahmadian, G., Liu, L., Becker, L.E., Sheng, M., and Wang, Y.T. (2000). Regulation of AMPA receptor-mediated synaptic transmission by clathrin-dependent receptor internalization. Neuron *25*, 649–662.

Murase, S., and Schuman, E.M. (1999). The role of cell adhesion molecules in synaptic plasticity and memory. Curr. Opin. Cell Biol. *11*, 549–553.

Murase, S., Mosser, E., and Schuman, E.M. (2002). Depolarization drives beta-Catenin into neuronal spines promoting changes in synaptic structure and function. Neuron *35*, 91–105.

Nuriya, M., and Huganir, R.L. (2006). Regulation of AMPA receptor trafficking by N-cadherin. J. Neurochem. *97*, 652–661.

Okamura, K., Tanaka, H., Yagita, Y., Saeki, Y., Taguchi, A., Hiraoka, Y., Zeng, L.H., Colman, D.R., and Miki, N. (2004). Cadherin activity is required for activity-induced spine remodeling. J. Cell Biol. *167*, 961–972.

Ozawa, M., Ringwald, M., and Kemler, R. (1990). Uvomorulin-catenin complex formation is regulated by a specific domain in the cytoplasmic region of the cell adhesion molecule. Proc. Natl. Acad. Sci. USA *87*, 4246–4250.

Phillips, G.R., Huang, J.K., Wang, Y., Tanaka, H., Shapiro, L., Zhang, W., Shan, W.S., Arndt, K., Frank, M., Gordon, R.E., et al. (2001). The presynaptic particle web: ultrastructure, composition, dissolution, and reconstitution. Neuron *32*, 63–77.

Racz, B., Blanpied, T.A., Ehlers, M.D., and Weinberg, R.J. (2004). Lateral organization of endocytic machinery in dendritic spines. Nat. Neurosci. *7*, 917–918.

Roura, S., Miravet, S., Piedra, J., Garcia de Herreros, A., and Dunach, M. (1999). Regulation of E-cadherin/Catenin association by tyrosine phosphorylation. J. Biol. Chem. *274*, 36734–36740.

Salinas, P.C., and Price, S.R. (2005). Cadherins and catenins in synapse development. Curr. Opin. Neurobiol. *15*, 73–80.

Spacek, J., and Harris, K.M. (1998). Three-dimensional organization of cell adhesion junctions at synapses and dendritic spines in area CA1 of the rat hippocampus. J. Comp. Neurol. *393*, 58–68.

Svoboda, K., Tank, D.W., and Denk, W. (1996). Direct measurement of coupling between dendritic spines and shafts. Science *272*, 716–719.

Takeichi, M., and Abe, K. (2005). Synaptic contact dynamics controlled by cadherin and catenins. Trends Cell Biol. *15*, 216–221.

Tanaka, H., Shan, W., Phillips, G.R., Arndt, K., Bozdagi, O., Shapiro, L., Huntley, G.W., Benson, D.L., and Colman, D.R. (2000). Molecular modification of N-cadherin in response to synaptic activity. Neuron *25*, 93–107.

Tang, L., Hung, C.P., and Schuman, E.M. (1998). A role for the cadherin family of cell adhesion molecules in hippocampal long-term potentiation. Neuron *20*, 1165–1175.

Tardin, C., Cognet, L., Bats, C., Lounis, B., and Choquet, D. (2003). Direct imaging of lateral movements of AMPA receptors inside synapses. EMBO J. *22*, 4656–4665.

Togashi, H., Abe, K., Mizoguchi, A., Takaoka, K., Chisaka, O., and Takeichi, M. (2002). Cadherin regulates dendritic spine morphogenesis. Neuron *35*, 77–89.

Triller, A., and Choquet, D. (2005). Surface trafficking of receptors between synaptic and extrasynaptic membranes: and yet they do move! Trends Neurosci. *28*, 133–139.

Uchida, N., Honjo, Y., Johnson, K.R., Wheelock, M.J., and Takeichi, M. (1996). The catenin/cadherin adhesion system is localized in synaptic junctions bordering transmitter release zones. J. Cell Biol. *135*, 767–779.

Wyszynski, M., Kim, E., Dunah, A.W., Passafaro, M., Valtschanoff, J.G., Serra-Pages, C., Streuli, M., Weinberg, R.J., and Sheng, M. (2002). Interaction between GRIP and liprin-alpha/SYD2 is required for AMPA receptor targeting. Neuron *34*, 39–52.

Yamagata, M., Sanes, J.R., and Weiner, J.A. (2003). Synaptic adhesion molecules. Curr. Opin. Cell Biol. *15*, 621–632.

Yu, X., and Malenka, R.C. (2003). Beta-catenin is critical for dendritic morphogenesis. Nat. Neurosci. *6*, 1169–1177.